2005 IEEE International Conference on Ultra-Wideband, 2005. ICU 2005. 5-8 Sept. 2005 Page(s):6 pp.

Characterization of the Ultra Wideband Body Area Propagation Channel

Andrew Fort[1,2], Claude Desset[1], Julien Ryckaert[1,2],
Philippe De Doncker[3], Leo Van Biesen[4], and Piet Wambacq[1,4,5,6]

[1]IMEC, Kapeldreef 75
B-3001 Leuven, Belgium
Email: forta@imec.be
+32.16.28.82.80

[3]ULB — Ondes et Signaux
CP 165/51 — Avenue Roosevelt 50
B-1050 Bruxelles, Belgium

[4]VUB — Dept. ETRO
Pleinlaan 2
B-1050 Brussel, Belgium

Abstract— **Using wireless sensors placed on a person to continuously monitor health information is a promising new application. In developing these sensors, detailed knowledge of the communication channel is essential. However, there are currently very few measurements describing propagation around the body. To address this problem, we have measured electromagnetic waves traveling near the torso to derive a simple pathloss law. The pathloss law is then extended to include the influence of arm movements and a surrounding office environment. This paper describes our measurement campaign and the basic characteristics of the body area radio channel.**

Keywords - **Propagation channel, ultra-wide band, body area network**

I. Introduction

Wireless bio-medical sensors is a promising new application made possible by recent advances in ultra low power technology. Each sensor measures parameters of interest and sends the data in short bursts to a central device such as a PDA. Examples include sensors to observe brain activity for recording or warning against seizure events, to examine heart activity for diagnosis and automatic emergency calls, to measure glucose levels in diabetic patients, and to monitor oxygen, blood pressure, or disease markers. The large diversity and potential of these applications makes it an exciting new research direction in wireless communications.

Ultra Wideband (UWB) [1] has recently received much attention as a promising air interface for short-range low data rate communication scenarios matching the requirements of wireless bio-medical applications [2, 3]. Furthermore, the FCC has recently legalized a spectral mask between 3.1-10.6 GHz specifically for UWB communication. Finally, the IEEE 802.15.4a committee is in the process of developing an UWB standard for ultra low power communication and has included body area networks (BANs) for medical and sport monitoring among their relevant application scenarios [4].

Unfortunately, there do not exist many measurements of the UWB body area channel required for low power bio-medical communication system design. Past attempts focused on simple Finite Difference Time Domain (FDTD) simulations for narrowband systems [5, 6] and UWB systems in the 3-6 GHz band [7]. However, due to the computational complexity of the FDTD method, simulations were limited to very simple scenarios that do not include the impact of a surrounding indoor environment or the impact of a small UWB antennas worn on the body. Narrowband measurements near the body in the 2.4 GHz band [8], as well as UWB measurements in the 3-6 GHz band [9–11] have also been reported. However, these studies do not describe the influence of arm motions, and provide only limited information about the impact of ground reflections and other nearby scatterers.

To address problems with body area channel characterization, we have measured electromagnetic wave propagation around the torso to develop a simple pathloss law and compared it with previous results in the literature. We then measure how the pathloss is influenced by simple arm motions. Finally, we measure the amount of energy received due to reflections off of the ground and surrounding scatterers in a typical office environment. We focus on the 3-6 GHz band which is an important portion of the UWB mask commonly proposed for UWB systems.

This paper discusses the results of our measurement campaign. Section II presents our measurement setup. Section III describes pathloss due to waves diffracting around the body and waves traveling along the front of the body. Section IV extends these results to include the influence of the arms on the pathloss. Section V describes the amount of energy received from reflections off the ground. Section VI discusses the influence of a surrounding office environment. Finally, section VII summarizes the major conclusions of this research.

II. Measurement Setup

UWB measurements are performed in the frequency range from 3 to 6 GHz. An HP8753ES vector network analyzer (VNA) is used to measure the S21 parameter between two antennas placed at various positions on a human body. The two antennas are connected to the VNA using 4 meter low-loss coaxial cables.

All measurements are made in a large empty room so that reflections off of the walls arrive later than the components diffracting around the body. The diffracting multipath components (MPCs) arrive at the receiver after 0.5-2

[2]Also PhD student at the Vrije Universiteit Brussel.
[5]Also lecturer at the Vrije Universiteit Brussel.
[6]This work was also supported by the MEDEA+ Witness Project.

ns depending on the position on the body. The earliest reflected MPCs are due to the ground and arrive after 8-10 ns. Reflections off the measurement setup (4 meters from the body) and surrounding walls (6 meters from the body) arrive considerably later. Therefore, reflected MPCs due to the surrounding environment can easily be identified and separated from propagation near the body.

The same small, low profile Skycross SMT-3TO10M [12] UWB antennas are used for all measurements. The antennas are 16 by 13.6 by 3 mm in size and weigh only 0.3 grams. These antennas were chosen since they accurately represent the kind of size and profile requirements typical of comfortable body worn sensor devices.

Measurements are taken between Skycross antennas worn on the body. We found that the distance between the body and the antenna has a dramatic influence on the pathloss and should be carefully controlled. We control the separation by either placing the antenna directly on the body, or putting a 5 mm dielectric between the body and the antenna. The antenna is then taped to this dielectric and held against the body using tight elastics so that they can not move while a measurement is being made.

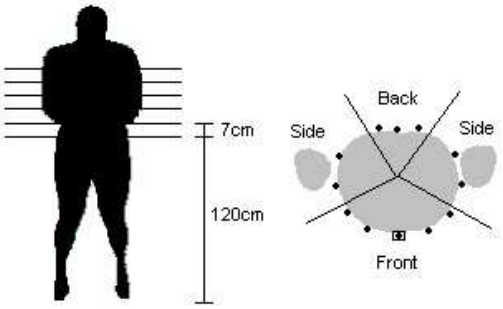

Fig. 1. Measurement locations on body (around the torso).

Figure 1 shows where the antennas are placed when measuring pathloss around the torso. All channel parameters are extracted from measurements performed in 6 planes separated by 7 cm along the vertical axis of the torso (see left diagram). The right diagram shows where the antennas are placed on the body for each plane. The receiver positions are marked with circles, while the transmitter position is marked with a box around the circle. The transmitter is always placed on the front of the body, and the receiver is placed at various positions on the torso at distances of 10 cm, 15 cm, 20 cm, 25 cm, 40 cm, and 45 cm measured around the perimeter of the body. To increase the number of points for extracting channel statistics, measurements one plane above and one plane below the transmitter are recorded at each distance. In this way, a total of 144 measurements are taken at various antenna positions.

We found that the channel parameters changed depending on the position around the body. To describe this phenomenon easily, we define three regions representing the front, side, and back of the body (see right diagram). The front region corresponds to observations taken between 0° to ±60°, the side region corresponds to observations taken between ±60° to ±160°, and the back region corresponds to observations taken between ±160° and ±180°.

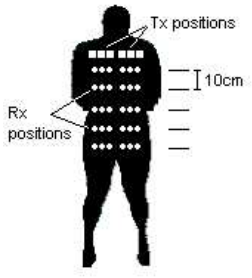

Fig. 2. Measurement locations on body (along the torso).

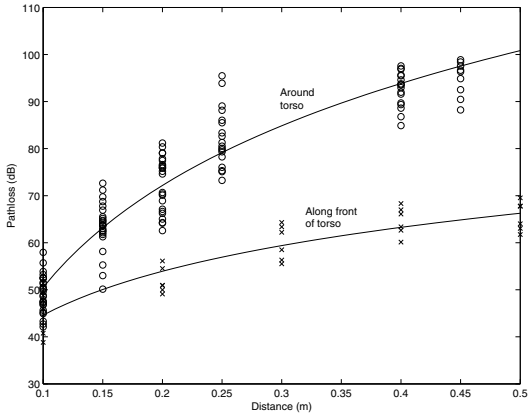

Fig. 3. Measured pathloss around the body. (Antennas are separated from the body by 5mm)

Figure 2 shows where the antennas were placed when measuring pathloss along the front of the body. The transmitter was worn at approximately shoulder height at one of six different positions. The receiver was placed directly below the transmitter at five positions separated by 10 cm.

III. Path Loss Model

FDTD simulations [7] have shown that paths traveling through the body in the GHz range are significantly attenuated. Instead, waves diffract around the torso. Therefore, we measure the distance around the perimeter of the body when modeling the path loss. This is in contrast to previous measurement campaigns in the GHz frequencies where the path loss model was erroneously assumed to be related to the straight-line distance through the body [9].

Figure 3 shows the path loss versus distance trend. The vertical axis represents the measured pathloss. The horizontal axis is the distance traveled by the wave along the perimeter of the body. The circles indicate individual measurements taken around the torso (figure 1). The crosses indicate individual measurements taken along the front of the torso (figure 2). It is clear that the path loss increases with distance as expected, and that there is a large variance around the mean pathloss. Furthermore, the pathloss due to diffraction around the body is higher than the pathloss due to waves traveling along the length of the body.

The pathloss is usually modeled with the following empirical power decay law:

$$P_{dB} = P_{0dB} + 10n \log(d/d_0) \qquad (1)$$

Parameter	*Around torso*	*Front of torso*
n	7.2	3.1
d_0	0.1 m	0.1 m
$P_{0dB}, 0mm$	57.5 dB	56.5 dB
$P_{0dB}, 5mm$	50.5 dB	44.6 dB

TABLE I
PATHLOSS MODEL PARAMETERS.

n is called the pathloss exponent, d is the distance from the antenna, d_0 is the reference distance, and P_{0dB} is the path loss at the reference distance. The parameters of this path model extracted from the measurements are shown in table I for the situation with the 5mm dielectric (P_{0dB}, 5mm) and without (P_{0dB}, 0mm).

The measured pathloss exponents are consistent with previous measurements and FDTD simulation results. In [7], a pathloss exponent of n = 7.4 for waves diffracting around the body between 2-6 GHz was estimated using an anatomically correct computer model of the human body. In [5], a pathloss exponent of n = 6 was estimated for narrowband systems operating in the 2.4 GHz around an elliptical container of salt water. In [9], a pathloss exponent of n = 3.3 was measured in an anechoic chamber for waves traveling along the front of the body in the 3-6 GHz range.

It is clear from figure 3 that there is a significant variance around the mean pathloss. It was shown in [7] that this variation is well described by a lognormal distribution. A maximum likelihood estimate (MLE) of the standard deviation of this distribution is $\sigma_{dB} = 3.6$ for transmission along the front of the body. For waves diffracting around the body, we observe slightly higher variation when the receiver was placed near the arms ($\sigma_{dB} = 7$) compared with when it it is placed on the front and back of the body ($\sigma_{dB} = 5$).

The reference pathloss depends on the separation between the antenna and the body due to antenna mismatches. As shown in table I, a significantly higher pathloss reference is measured when the antenna is placed directly on the torso (P_{0dB}, 0 mm separation) compared with when it is placed 5 mm away from the torso (P_{0dB}, 5 mm separation). It is therefore possible that a body-aware antenna design could improve system performance in scenarios where the sensor must be worn directly on the body.

Several UWB studies have proposed a frequency dependent pathloss model [13, 14]. To test for frequency dependency, we have measured the pathloss separately in six 500 MHz sub-bands between 3 GHz to 6 GHz. We do not observe any significant variation in the pathloss versus frequency on average. However, some frequency dependency is observed for individual measurements consistent with results reported in [11].

IV. Influence of the arms

We use the same setup as in section II to measure the influence of arm motions on the pathloss. The transmitter is placed on the front of the body, and the receiver is placed on either the front, side, or back of the body at a distance of 10 cm, 20 cm, and 45 cm respectively (see figure 1). The arms are then moved to the front or side of the body in increments of 10 degrees as shown in figure 4. At each arm position, the received power is recorded to determine the influence of the arms. For each distance, the experiment is repeated three times in different planes along the torso to ensure reproducible results.

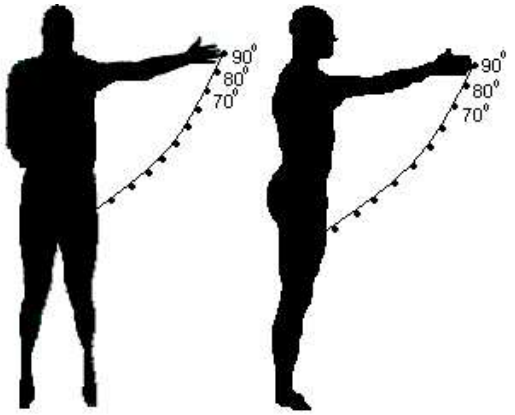

Fig. 4. Measured arm movements to the side of the body (left) and to the front of the body (right)

A. Receiver on the front of the body

Figure 5 shows three-dimensional plots representing the received power versus time for arm motions to the front and side of the body. The z-axis is the received power, the x-axis is time, and the y-axis shows the arm position from 0° to 90° as demonstrated in figure 4. Power versus time plots are obtained by taking the inverse Fourier Transform of the S21 parameter in a similar manner as in [9].

Figure 5(a) shows that arm motions to the side do not significantly alter the received power versus time when both antennas are located on the front of the body. Clearly, the arms are too far away to have any impact and therefore can be ignored.

Conversely, 5(b) shows that if the arms are in front of the body, the received power versus time changes as a function of the arm position. Specifically, a reflection off the arms can be seen when they are positioned between $40° - 70°$ in front of the body. As expected, the reflection arrives earlier when the arms are moved toward the torso. When the arms are located near the side, the reflection is no longer observed.

It is possible to exploit the reflections off of arms in front of the body using a RAKE receiver. However, they are not reliable enough features for communication since we can not guarantee that the arm will be in front of the body for most application scenarios.

While the typical arm movements we have described so far do not dramatically influence the pathloss, we found that the arms can significantly influence the received energy if they are moved such that they shadow the line of sight path between the transmitter and receiver. For example, when the transmitter is placed on the belt, and the receiver is placed near shoulder height, a drop between 5-20 dB in received energy is recorded when the arms are folded across

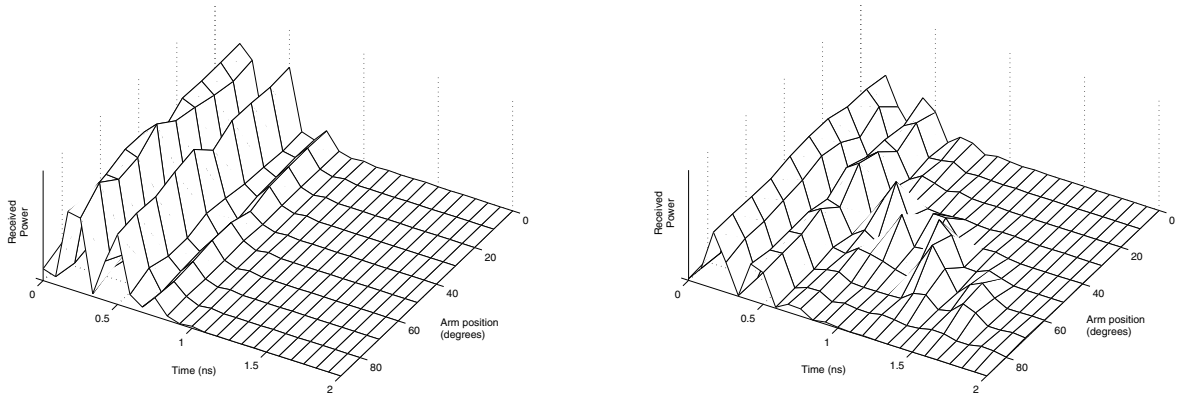

(a) Arm motion to the side of body

(b) Arm motion to the front of the body

Fig. 5. Received power when receiver is on the front of the body.

the chest between the two antennas. The variation depends on the position of the antennas and arms. Therefore, UWB biomedical systems located on the front of the body may need to account for the possibility of deep fades due to arm movements blocking transmission.

B. Receiver on the side or back of the body

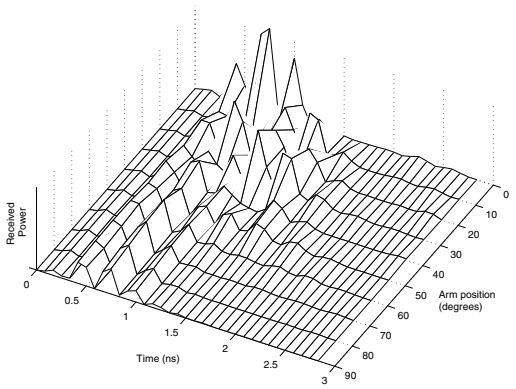

Fig. 6. Received power when receiver is on the side of the body. Arm motion to the side of the body.

Figure 6 shows the influence of a sideway arm motion when the receiver antenna is worn on the side of the body. When the arms are far away from the body, between $50° - 90°$, they have no influence on the received power. However, when the arms are moved closer to the side of the body, reflections are observed. These reflections interfere with the initial diffracting wave causing fluctuations in the received power as seen in figure 6. Similar behavior is also observed when the receiver is placed on the back of the body.

The power fluctuation due to a body in motion has been compared with the fluctuation due to a still body to more accurately describe the statistical variation. As before, the transmitter is placed on the front of the body, and the receiver is placed at several positions along the front, side, and back. For each antenna position, 100 measurements are made while the person stands still. This is followed by 100 measurements while the person walks in place with a swinging motion of the arms.

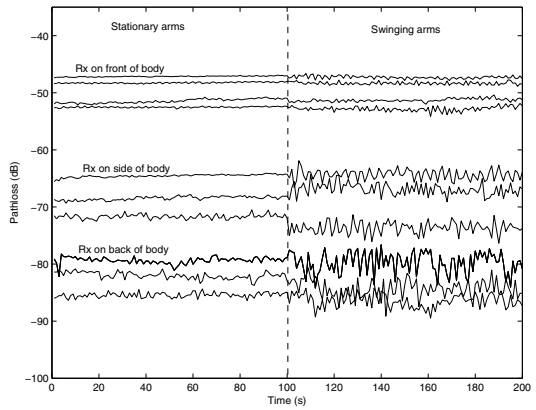

Fig. 7. Received power fluctuations of a body standing still and a body in a walking motion.

Figure 7 summarizes the results for both no motion and a walking motion. Each line shows the pathloss versus time for a different transmitter and receiver position. As expected, there is only a negligible power variation while the body is still regardless of the antenna position. However, a walking motion produces measurable fluctuations if the receiver is placed on the side or back of the body.

Fluctuations around the mean path loss at each position have been extracted and several distrubtions fit to the resulting data including the Lognormal, Nakagami-m, and Rayleigh distributions. Only the lognormal and Nakagamim distributions provide a plausible fit. The Rayleigh distribution can be rejected based on visual inspection of the empirical and fit distributions, and because it fails the χ^2 goodness of fit test with less than a 1% significance level. In general, the Rayleigh fading model is grossly pessimistic.

ML estimates of the lognormal mean and variance are summarized in table II. These variances are smaller than the variance around the mean pathloss in section III indicating that the position of the antennas on the body has a more significant impact on received power than typical arm motions, provided the arms don't shadow the receiver.

Receiver Position	μ_{dB}	σ_{dB}
Front	-0.01	0.3
Side	-0.14	1.1
Back	-0.27	1.5

TABLE II
DISTRIBUTION OF RECEIVED ENERGY FLUCTUATION DUE TO ARM MOTIONS

V. GROUND REFLECTIONS

We use the same setup as in section II to measure reflections off of the ground. The transmitter is placed on the front of the body, and the receiver is placed at several positions around the torso as in figure 1. All measurements are made in a semi-anechoic chamber with a non-absorbing floor so that we observe only the component diffracting around the body and the ground reflection (see figure 8).

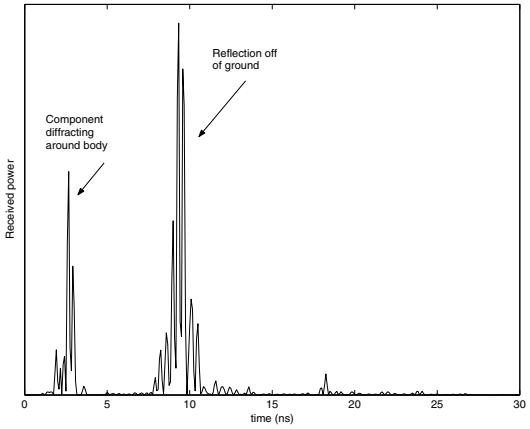

Fig. 8. Ground reflection recorded in a semi anechoic chamber (receiver on back of body).

The ground reflection clearly seen in figure 8 was also reported in FDTD simulations [7] and past measurement campaigns [9,10]. This is an important component to study because it is always present, even in outdoor scenarios when there are no other nearby scatterers. Therefore, it is a reliable feature of the channel that could be exploited by an UWB receiver.

The magnitude of the reflection is approximately log-normally distributed depending on the position of the antenna on the torso. Very little correlation (ρ between 0.2 to 0.35) is measured between the log magnitude of the ground reflection and the diffracting wave consistent with FDTD results reported in [7]. ML estimates of the lognormal mean (μ_{dB}) and standard deviation (σ_{dB}) are provided in table III.

Receiver Position	μ_{dB}	σ_{dB}
Front	-82.7	3.2
Side	-87.0	2.9
Back	-93.2	3.5

TABLE III
DISTRIBUTION OF RECEIVED ENERGY REFLECTED FROM GROUND

The dB units in table III are relative to the transmitted energy and can therefore be compared directly with the pathloss results from figure 3. It is clear that when both antennas are placed on the front of the body, the floor reflection is very small compared with the diffracting wave and can be ignored. However, when the receive antenna is placed on the side or the back of the body, the floor reflection becomes more important as the diffracting wave is significantly attenuated. In fact, on the back of the body, the floor reflection is often larger than the diffracting wave despite traveling a longer distance. This is consistent with the observations from section III that waves traveling along the length of the body have a lower pathloss exponent compared with waves diffracting around the body.

VI. REFLECTIONS FROM THE SURROUNDING ENVIRONMENT

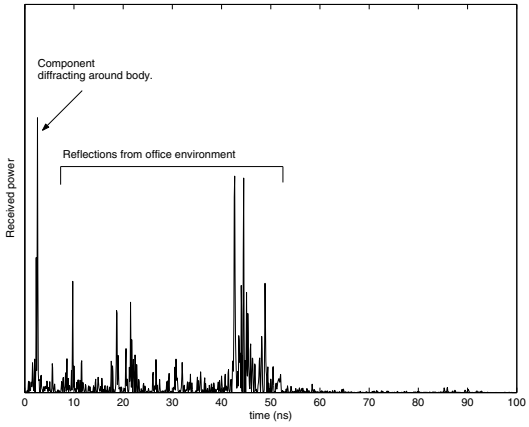

Fig. 9. Office environment reflections (receiver on back of body).

We use the same setup as in section II to measure the influence of the surrounding office environment. The transmitter is placed on the front of the body, and the receiver is placed on either the front of the body (10 cm distance), the right side of the body (20 cm distance), or the back of the body (45 cm distance) as in figure 1. The S21 parameter is measured at several positions around a 3.7 by 6.1 by 2.8 meter office, and then converted to the time domain using an inverse Fourier Transform.

Figure 9 shows an example of the received power versus time at one position in the room when the receiver is worn on the back of the torso. In addition to the component diffracting around the body, several later multipath components are observed due to reflections off of surrounding scatterers. By integrating the energy received after the arrival of the diffracting wave, we obtain the total average energy received due to MPCs reflecting off of the surrounding environment and arriving back at the body. Table IV shows the ML estimate of the lognormal mean (μ_{dB}) and standard deviation (σ_{dB}) of the reflected energy normalized to the transmitted energy for each side of the body.

Clearly, more energy is reflected from the surrounding environment when the antennas are placed on the same side of the body compared with when the antennas are placed on different sides of the body. Signal components arriving at the receiver on a different side of the body may take

Receiver position	μ_{dB}	σ_{dB}
Front	-69.1	0.9
Side	-72.6	3.1
Back	-77.5	2.5

TABLE IV
DISTRIBUTION OF RECEIVED ENERGY REFLECTED FROM INDOOR ENVIRONMENT.

longer and more indirect paths since many of the nearby scatterers become partially shadowed by the body. Thus, it is not surprising that the received reflected energy is lower on average. Similarly, we observe a larger variance when the receive antenna is shadowed by the body because the signal paths likely undergo additional reflections.

As expected, comparing table IV with table III indicates that more reflected energy is received in an office full of scatterers compared with in an semi-anechoic chamber having only the floor reflection.

Comparing table IV with figure 3 shows that if the antennas are placed on the same side of the body, the received energy due to MPCs reflecting off of nearby scatterers is significantly smaller than the energy received due to MPCs propagating near the body and can be ignored. However, if antennas are placed on different sides of the body, the total energy of reflected components becomes very important as the initial diffracting wave is significantly attenuated. Reflected energy may also be important when the transmitting and receiving antennas are shadowed by the arms as discussed in section IV-A.

A complete analytical description of the indoor body area channel response is beyond the scope of this paper, but we can briefly summarize a few results. When the receiver is placed on the back of the body, the average rms delay spread is approximately 33 ns and an average of 20 individual MPCs within 10 dB of the strongest component are observed. This indicates that the available energy is spread over a relatively long excess delay. While simple receiver designs will benefit from these components, more complex RAKE receivers would be needed to fully exploit the available energy.

VII. Conclusions

Using sensors to monitor health information around the body is a promising new wireless application. Furthermore, emerging UWB technologies provide a potential air interface for low data rate short range communication scenarios matching the requirements of bio-medical sensor devices. Unfortunately, there are very few measurements describing the the radio propagation channel required for communication system design. This paper outlines the basic characteristics of the body area channel based on an extensive measurement campaign. The pathloss of waves diffracting around the body is shown to be much higher than waves traveling along the front of the body. The reference pathloss near the antenna depends on the separation between the antenna and the body due to antenna mismatch. This mismatch indicates that a body-aware antenna design could improve system performance in scenarios where the sensor must be worn directly on the body. Further, arm motions to the front and side of the body can have a small impact on the received power. More significant variations are recorded when the arms are moved so that they shadow the line of sight between the two antennas. In addition to components diffracting around the body, a deterministic floor reflection is also observed. By comparing the distribution of the received energy of the floor reflection with the energy of waves diffracting around the body, we find the reflection becomes very important when the receiver is placed on a different side of the torso from the transmitter. Finally, a significant amount of energy is measured due to reflections from objects in a surrounding office environment. This energy could be exploited by the receiver to improve system performance.

Acknowledgment

The authors would like to thank Professor Pierre Degauque and Martine Liénard from the Université des Sciences et Technologies de Lille (USTL) for allowing us to use the anechoic chamber and helping us in making these measurements.

References

[1] Win M. Z. and Scholtz R. Impulse radio: How it works. In *IEEE Communications Letters*, February 1998.
[2] R. Shmidt et al. Body area network, a key infrastructure element for patient-centered medical applications. *Biomed. Tech (Berl)*, 47:365–368, 2002.
[3] B. Gyselinckx, C. Van Hoof, S. Donnay. Body area networks, the ascent of autonomous wireless microsystems. In *International Symposium on Hardware Technology Drivers of Ambient Intelligence*, 2004.
[4] IEEE 802.15.4a. http://www.ieee802.org/15/pub/TG4a.html.
[5] I. Moerman L. Martens F. Louagie S. Donnay B. Latre, G. Vermeeren and P. Demeester. Networking and propagation issues in body area networks. In *Proceedings SCVT*, 2004.
[6] Julien Ryckaert, Ph. De Doncker, Stephane Donnay, Arnaud Delehoye, and R.Meys. Channel model for wireless communication around the human body. In *Electronics letters*, volume 40, pages 543–544, April.
[7] Andrew Fort, Claude Desset, Julien Ryckaert, Philippe DeDoncker, Leo Van Biesen, and Stephane Donnay. Ultra wideband body area channel model. In *ICC Proceedings*, Seoul, Korea, 2005.
[8] P. Hall, M. Ricci, and T. Hee. Measurements of on-body propagation characteristics. In *International Conference on Microwave and Millimeter Wave Technology*, pages 770–772, 2002.
[9] T. Zasowski, F. Althaus, M. Stager, A. Witttneben, and G. Trőster. UWB for noninvasive wireless body area networks: channel measurements and results. In *2003 IEEE Conference on Ultra Wideband Systems and Technologies*, pages 285–289, 2003.
[10] Istvan Z. Kovacs, Gert F. Pedersen, Patrick C.F. Eggers, Kim Olesen. Ultra wideband radio propagation in body area network scenarios. In *ISSSTA Proceedings*, pages 102–106, 2004.
[11] Kovacs I.Z. and Eggers P.C.F. Technical deliverable D4.2: UWB radio channel characterisation for portable user terminal scenarios. Technical report, October 2004.
[12] Skycross. http://www.skycross.com.
[13] J. Kunisch and J. Pamp. Measurement results and modeling aspects for the UWB radio channel. In *IEEE Transactions on Vehicular Technology*, pages 1204–1316, 1999.
[14] A. Alvarez, G. Valera, M. Lobeira, R. Torres and J.L. Garcia. New channel impulse response model for UWB indoor system simulations. In *Proceedings VTC 2003 spring*, volume 138, pages 1204–1316, 1999.